ACS APPLIED MATERIALS & INTERFACES

Research Article

www.acsami.org

Effective Electrocatalysis Based on Ag_2O Nanowire Arrays Supported on a Copper Substrate

Rong Ji, Lingling Wang, Liutao Yu, Baoyou Geng, Guangfeng Wang,* and Xiaojun Zhang*

College of Chemistry and Materials Science, Anhui Normal University, Wuhu 241000, People's Republic of China
Key Laboratory for Functional Molecular Solids of the Education Ministry of China, Wuhu 241000, People's Republic of China
Anhui Key Laboratory of Chem-Biosensing, Anhui Normal University, Wuhu 241000, People's Republic of China

Supporting Information

ABSTRACT: Silver oxide nanowire arrays (Ag_2O NWAs) were first synthesized on a copper (Cu) rod by a simple and facile wet-chemistry approach without using any surfactants. The as-synthesized Ag_2O NWA/Cu rod not only can be used as an integrated electrode (called a Ag_2O NWA/CRIE) to detect hydrazine (HZ) but also can serve as the catalyst layer for a direct HZ fuel cell. The current density of HZ oxidation on Ag_2O NWA (94.4 mA cm^{-2}) is much bigger than that on a bare Cu rod (3.9 mA cm^{-2}) at −0.6 V, and other Ag_2O NWAs have the lowest onset potential (−0.85 V). This suggests that a Ag_2O NWA integrated electrode has potential application in catalytic fields that contain the HZ fuel cell.

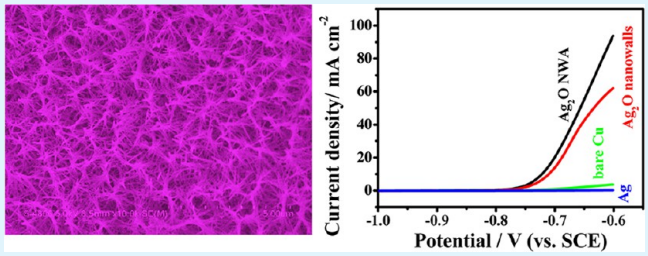

KEYWORDS: *silver oxide, integrated electrode, hydrazine, amperometric sensor, electrocatalysis*

1. INTRODUCTION

Nanowires, nanobelts, and nanotubes of metal/metal oxide as typical one-dimensional (1D) nanoscaled materials have received special attention because of their peculiar physical, chemical, and electrical properties and other potential applications.[1−12] Ag_2O as a p-type semiconductor with a band-gap energy of about 1.46 eV has aroused much attention because of its high catalytic activity as well as its selectivity as a catalyst.[13−15] Up to now, much effort has been spent on the preparation of Ag_2O nanostructures including nanorods, nanoparticles, and nanoctahedra[16−21] by various methods, including electrodeposition, laser-induced fragmentative decomposition, a hydrothermal method, and so on.[16,22,23] However, the reaction processes of those methods are complicated or need high temperature; a simple method to synthesize Ag_2O nanostructures is indispensable. It is well-known that Ag_2O nanowire arrays (NWAs) have large surface areas, which can make them useful in diverse applications such as catalyst and chemical sensors, but to the best of our knowledge, there is no record of Ag_2O NWAs called 1D nanostructures. Hence, the development of a simple Ag_2O NWA synthetic method is meaningful.

Hydrazine (HZ) is toxic and probably even mutagenic; therefore, credible and sensitive analytical methods are needed to detect the concerntration of HZ. We all know that electrochemical techniques are portable, inexpensive, and sensitive methodologies.[24−32] An Ag_2O NWA/Cu rod used as an integrated electrode (Ag_2O NWA/CRIE) was confirmed to detect HZ sensitively; this can be supported by the results of electrochemical techniques. However, everything is a double-edge sword; as a candidate of fuels for a fuel cell, HZ also has been researched because of its high energy density. Besides that, it is a low-cost material, and the method of synthesis is relatively simple. Many aspects of a direct HZ air fuel cell are superior to those of other conventional fuel cells, such as a higher theoretical electromotive force (E^{θ} = 1.62 V), a higher energy density (E = 5.419 h g^{-1}), and a near-ambient working temperature;[33] it received an in-depth study in recent years. The electrochemical oxidation of HZ in an alkaline solution produces four electrons, and the total reaction of the HZ fuel cell is[34]

$$N_2H_4 + OH^- \rightarrow N_2H_3 + H_2O + e^- \quad \text{(slow)}$$

$$N_2H_3 + 3OH^- \rightarrow N_2 + 3H_2O + 3e^- \quad \text{(fast)}$$

The first HZ fuel cell was researched more than 40 years ago;[35] HZ oxidation on nickel,[36,37] palladium,[38,39] platinum,[40,41] cobalt,[42] gold,[43,44] silver,[44] and mercury[45] electrodes in alkaline media was intensively investigated from the 1960s to the 1980s, but it has attracted renewed interest in the last few years[46−52] mainly because of the enhanced cost of oil and incremental demand for stationary and mobile applications, including vehicles. However, there is still the problem of a lack of mass production, and a further research is required.

The goal of this work was to develop a new nanostructured Ag_2O. Then we studied the high electrocatalysis for HZ

Received: May 4, 2013
Accepted: August 26, 2013
Published: August 26, 2013

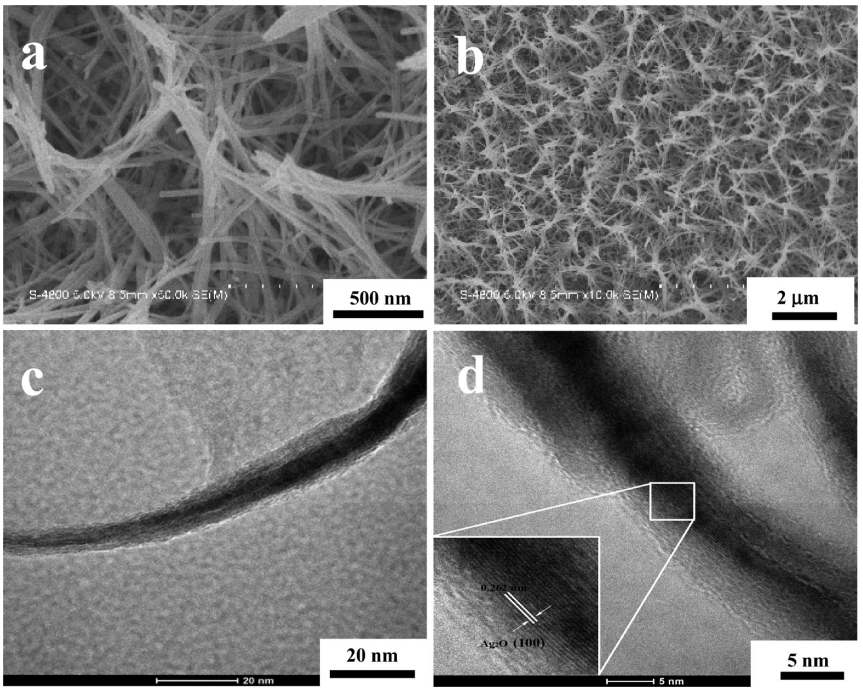

Figure 1. (a) High-magnification and (b) low-magnification SEM images of Ag_2O NWAs. (c) TEM image of Ag_2O NWAs. (d) HRTEM image of Ag_2O NWAs. Inset: Expanded view of the areas enclosed by the white rectangles.

detection as well as the HZ fuel cell. Previously, we used the adsorption method to make nanomaterials loaded onto conductive substrates for practical applications. Considering that these nanomaterials may degrade over the long term, the activation area could be decreased. Making the nanomaterials and substrates a whole integration was the strategy, so we used a simple method to synthesize Ag_2O NWAs on a Cu rod. An integrated electrode could be used in the electrochemical oxidation of HZ. We also confirmed that it possesses underlying application for the HZ fuel cell.

2. EXPERIMENTAL SECTION

2.1. Preparation of Ag_2O NWA/CRIE. A Cu rod (cross section = 2.5 mm^2; length = 4 cm) was cleaned from a consecutive ultrasonication in acetone, ethanol, and distilled water, the water was removed from the surface of the Cu rod and dipped into a test tube containing a 0.01 M $AgNO_3$ aqueous solution, then 0.1 M NaOH was added to the reaction system, and the tube was sealed and maintained for 12 h at room temperature. In order to remove the impurities before characterization, the product was washed for several times using distilled water and ethanol (the volume ratio of the two solutions was 1:1).

2.2. Characterization and Measurements. The Ag_2O nanomaterials were characterized by various techniques. The morphologies of the Ag_2O NWAs were characterized by scanning electron microscopy (SEM; Hitachi S-4800) and field-emission transmission electron microscopy (TEM; JEOL 2010). Powder X-ray diffraction (XRD) patterns of the as-prepared materials were recorded on a Shimadzu XRD-6000 instrument employing a scanning rate of 0.05° s^{-1} with the 2θ range from 10° to 80°, with high-intensity Cu Kα radiation (λ = 0.154178 nm). Energy-dispersive X-ray (EDX) spectroscopy was used to analyze the elements. Electrochemical measurements were tested on a CHI 760D electrochemical workstation with a conventional three-electrode system at room temperature. The Ag_2O NWA/CRIE, saturated calomel electrode (SCE), and coiled platinum wire electrode were applied as the working electrode, reference electrode, and auxiliary electrode, respectively. All reported potentials are relative to SCE. Cyclic voltammetry (CV) and scanning electron microscopy were carried out in an aqueous solution of 0.1 M NaOH. Linear sweep voltammetry (LSV) was implemented in a mixed solution that contained 3 M NaOH and additional 1 M N_2H_4.

3. RESULTS AND DISCUSSION

3.1. Structural Characterization of Ag_2O NWAs. As presented in Figure 1a,b, Ag_2O NWA is densely covered on the Cu substrate with lengths in the range of 2−10 μm. TEM images of the as-prepared sample (see Figure 1c,d) revealed 1D wire structures with widths of 10−30 nm. A high-resolution TEM (HRTEM) image showed that the Ag_2O nanowires are single crystals; the lattice distance is about 0.262 nm, which is close to 0.266 nm, the interplanar distance of {100} facets (see Figure 1d and inset).

According to the reported date (JCPDS card no. 75-1532), all of the major diffraction peaks located at (111), (200), (220), and (311) in the XRD pattern (see Supporting Information Figure S1a) can be indexed to the monoclinic Ag_2O phase with lattice constants and no detectable impurity phase is found. By the way, some diffraction peaks of Cu still exist because the materials were synthesized on a Cu rod. We used X-ray photoelectron spectroscopy (XPS) techniques to further characterize the components of our materials; the results are shown in Figure S1b in the Supporting Information. The curve is a typical peak of Ag 3d. Figure S2 in the Supporting Information is the corresponding EDX result of Figure 1b; it shows that the silver and oxygen contents dominate in the Ag_2O nanomaterial. Meanwhile, a small amount of gold also exists because we steamed gold onto the samples before we tested them. In addition, the peaks at 8 and 9 keV are due to the use of a Cu rod.

3.2. Factors Influencing the Formation of the Ag_2O NWAs. The selection of the reaction time is crucial for the formation of such Ag_2O NWAs. In addition, the concentration of $AgNO_3$ in the precursor solution and the concentration of

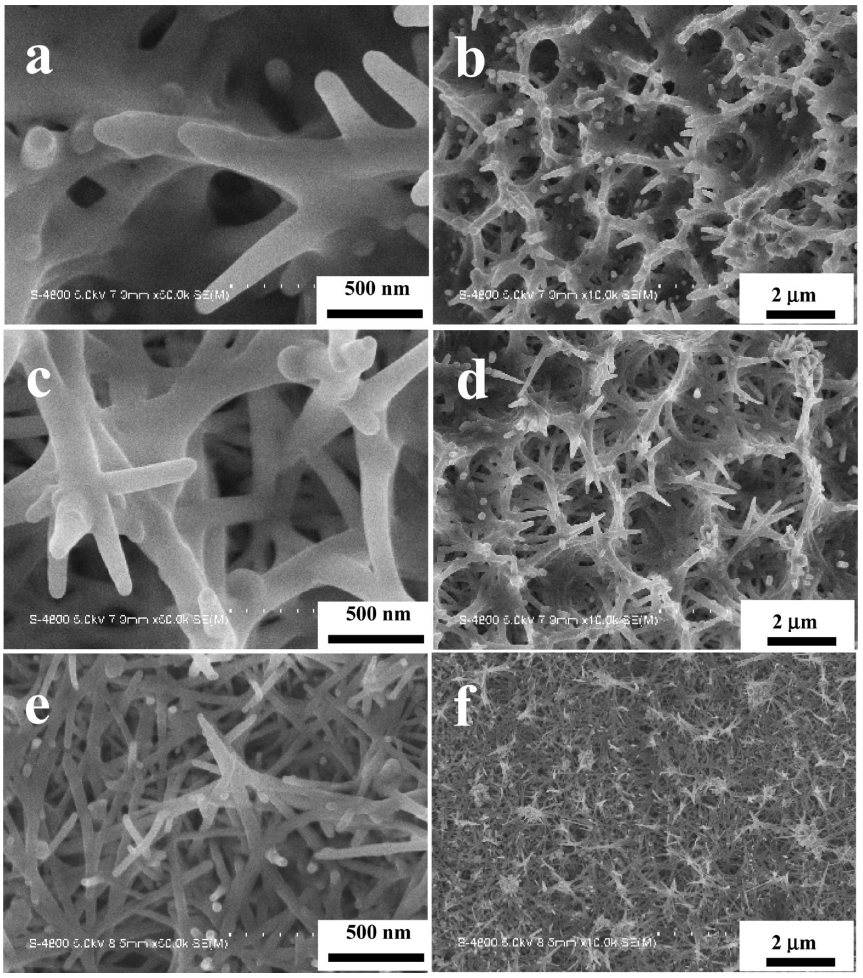

Figure 2. Typical SEM images of products obtained at different periods: (a and b) 2 h; (c and d) 6 h; (e and f) 24 h.

NaOH are also important to the morphologies of the final products.

3.2.1. Influence of the Reaction Time. It has been known that the reaction time is a critical parameter for the vegetation process of the Ag_2O NWAs. In Figure 2a,b, we can see that only sparse and short nanowires are formed on a layered film when the reaction time is 2 h. According to our previous work,[53] when the concentration of $AgNO_3$ was 0.01 M, dendritic silver quickly formed on the Cu rod. So, we identified that the layered film consisted of silver based on former work and the EDX pattern (see Figure S3 in the Supporting Information). When the time was raised to 6 h, lots of nanowires formed on the substrate, but they were not uniform and the silver layered film became thinner because of oxidation of silver in alkaline media (see Figure 2c,d). Then the dense and long NWAs formed and the layer disappeared (Figure 1a,b) when the reaction time reached 12 h. When the reaction time was prolonged to 24 h, nanowires became wider and stacked together (see Figure 2e,f).

3.2.2. Influence of the Ag^+ Concentration in the Precursor Solution. Figure 3 shows the morphologies of the products synthesized with different concentrations of Ag^+ in the precursor solution. When the concentration was 0.001 M, nanowires and lots of irregular nanoparticles appeared (Figure 3a,b). The XRD pattern (see Figure S4 in the Supporting Information) of the product under this reaction parameter showed that the product was $Cu(OH)_2$, not Ag_2O. A possible interpretation is that the concentration of Ag^+ is too low, and the Ag layer cannot form in such a short time. When the NaOH solution was added, Ag^+ reacted with OH^- and formed Ag_2O precipitation first, and then the rest of the NaOH reacted with the Cu rod. When the Ag^+ concentration was increased to 0.05 M, silver nanodendritics and nanoparticles formed (see Figure 3c,d). This demonstrated that the Ag^+ concentration was too high, consuming OH^- quickly and forming Ag_2O precipitate in the solution, and then the rest of the Ag^+ reacted with the Cu rod. If the Ag^+ concentration reached up to 0.1 M, as shown in Figure 3e,f, the morphologies of the obtained products were similar to those in Figure 3c,d.

3.2.3. Influence of the Concentration of NaOH. Figure 4 shows the morphologies of the products synthesized from the solution ($[Ag^+]$ = 0.01 M) with different NaOH concentrations. When the concentration was 0.01 M, no Ag_2O nanowires were found in the silver layer grown on the Cu rod. This is due to the low concentration of NaOH; Ag^+ was selected to increase the replacement reaction with the Cu rod. As a result, the final product is silver (see Figure 4a,b). After the addition of 0.5 M NaOH, we can see (see Figure 4c,d) that the nanowires became thicker than that when 0.1 M NaOH was added (see Figure 1a,b). If the concentration of NaOH continued to increase to 2 M, the Ag_2O NWAs not only become thicker but also aggregated together (see Figure 4e,f). This was due to the high concentration of NaOH and led to a fast reaction speed, thereby forming thicker nanowires produced and aggregated together.

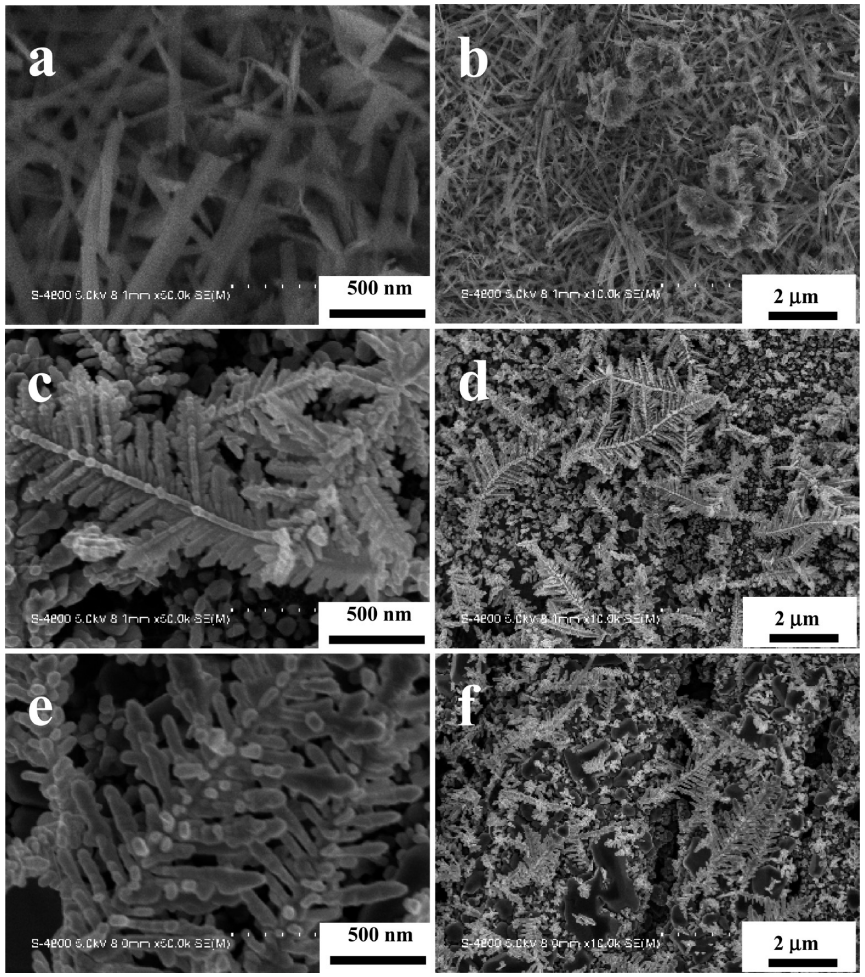

Figure 3. Typical SEM images of products obtained at different concentrations of $AgNO_3$: (a and b) 0.001 M; (c and d) 0.05 M; (e and f) 0.1 M.

3.2.4. Formation of Ag_2O NWAs. As a result of the silver layered film that formed in the beginning of the reaction and then disappeared, we believe that the silver layered film has a vital function in generation of the silver oxide nanowire process. In order to prove this conception, the same volumes of 0.01 M $AgNO_3$ and 0.1 M NaOH were mixed first, and then the Cu rod was dipped into the test tube and maintained at room temperature for 12 h. The results showed that some nanowires and nanoparticles coexisted on the surface of the Cu rod (see Figure S5 in the Supporting Information). The EDX pattern identified that the product was not Ag_2O (Figure S6 in the Supporting Information), which indicated that a copper oxide nanowire may have formed in a redundant alkaline solution and so could not have formed a silver layer first. In order to prove that copper oxide nanowire could not have formed in a surplus alkaline solution after the silver layer formed, we changed the reaction time of the optimal experiment to 24 h; other reaction parameters were all according to optimum conditions. The product was characterized by XRD, as shown in Figure S7 in the Supporting Information. All of the major diffraction peaks were also indexed to the monoclinic Ag_2O phase. Therefore, we think the formation mechanism of the Ag_2O nanowire is as follows:

$$Ag^+(sol) + Cu(s) = Ag(s) + Cu^{2+}(sol) \quad (1)$$

$$Ag^+(sol) + OH^-(sol) \Leftrightarrow Ag(OH)(s) \quad (2)$$

$$4Ag(s) + O_2 + 4OH^-(sol) = 4Ag(OH)(s) + 2H_2O \quad (3)$$

$$2Ag(OH)(s) \Leftrightarrow Ag_2O(s) + H_2O \quad (4)$$

3.3. Detection of HZ. The produced integrated electrode was used to directly detect HZ in solution. As shown in Figure 5a, it exhibits an obvious anodic current increment on Ag_2O NWA/CRIE near 0.37 V, which is due to oxidation of HZ. However, the response of HZ for the bare Cu rod and the product in Figures 2a,b and 4e,f was so weak (see Figure S8 in the Supporting Information). These results demonstrated the catalytic effects of Ag_2O NWA/CRIE toward the efficient oxidation of HZ. The influence of the scanning rates on the cyclic voltammogram response of Ag_2O NWA/CRIE in 0.1 M NaOH was also evaluated (see Figure 5b). It shows that the Ag_2O NWA/CRIE anodic peak current increased when the scanning rates ranged from 50 to 150 mV s^{-1}. The inset of Figure 5b is the corresponding calibration curve and linear plot of the peak current (I_p) versus the scanning rates on Ag_2O NWA/CRIE. The peak current I_p is proportional to scanning rate ν, signifying the dominance of the adsorption process. According to the equation[54]

$$I_p = \frac{n^2F^2\nu A\Gamma_c}{4RT}$$

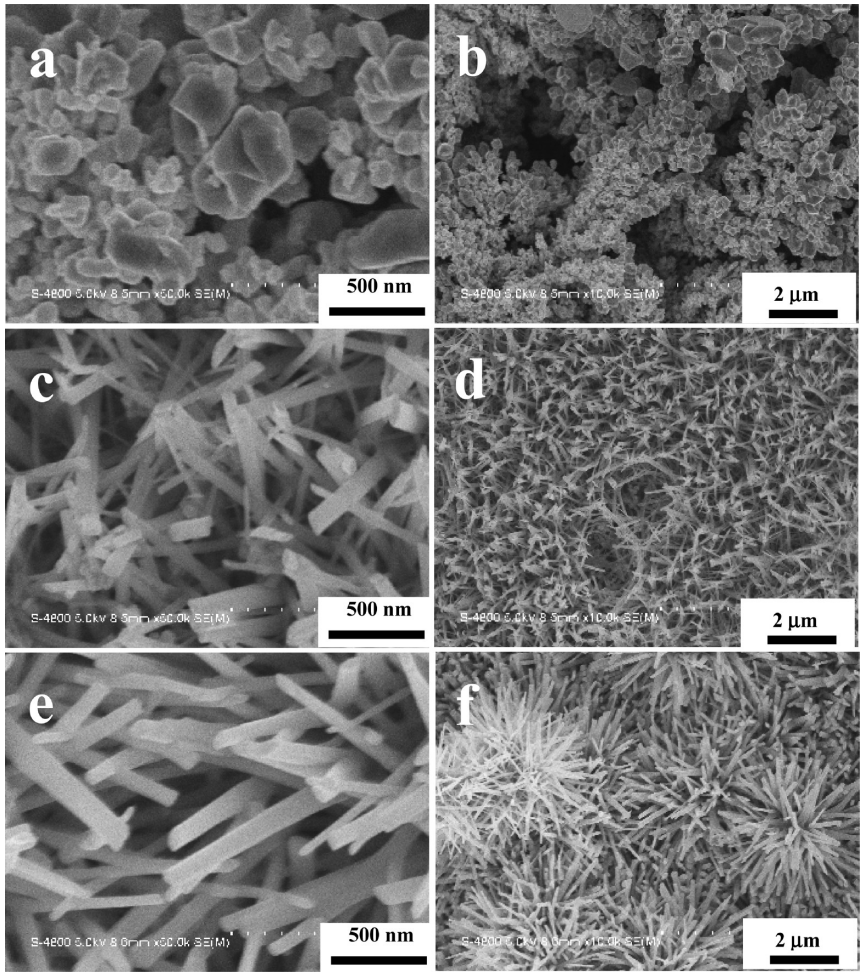

Figure 4. Typical SEM images of the products obtained at different concentrations of NaOH: (a and b) 0.01 M; (c and d) 0.5 M; (e and f) 2 M.

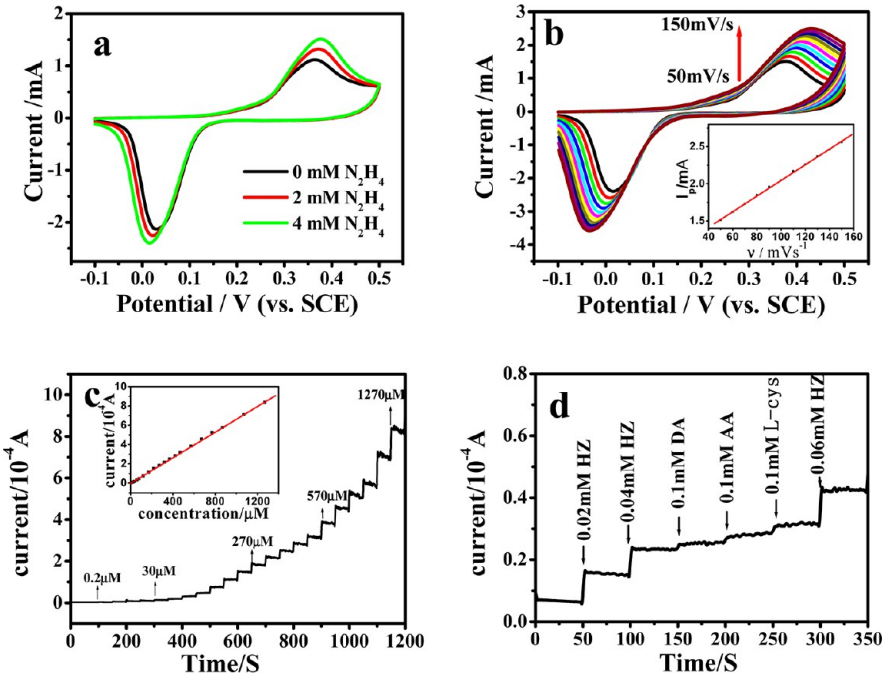

Figure 5. (a) Cyclic voltammograms of Ag_2O NWA/CRIE in 0.1 M NaOH with different concentrations of HZ at a scanning rate of 50 mV s^{-1}. (b) Cyclic voltammograms of Ag_2O NWA/CRIE in 0.1 M NaOH containing 4 mM HZ at different scanning rates. Inset: corresponding calibration curve and linear plot of the peak current (I_p) versus the scanning rates for Ag_2O NWA/CRIE.

dx.doi.org/10.1021/am4016523 | ACS Appl. Mater. Interfaces 2013, 5, 10465−10472

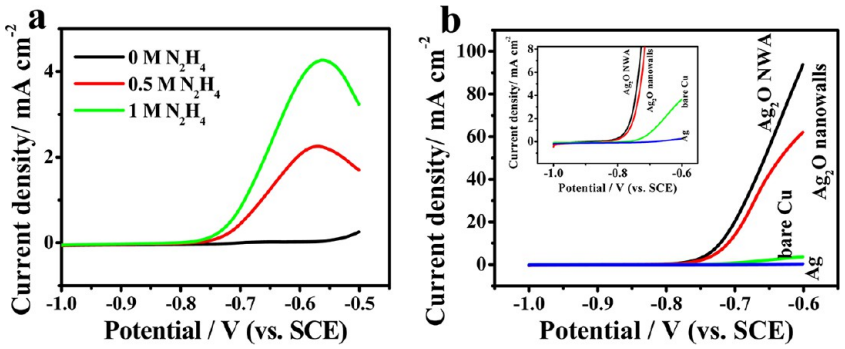

Figure 6. (a) LSV curves of a bare Cu electrode in 3 M NaOH with 0 M, 0.5 M, and 1 M HZ. (b) LSV curves of electrooxidation of HZ for Ag_2O NWAs, Ag_2O nanowalls, a bare Cu, and ordinary silver electrodes at a scanning rate of 50 mV s^{-1}. Inset: corresponding magnified curves.

where I_p was the peak current, A is the electrode surface area, and the other symbols have their usual meanings, the surface coverage concentration τ_c for Ag_2O NWA/CRIE was calculated to be 3.68×10^{-8} mol cm^{-2}. The surface coverage of the copper hydr(oxide) layer on the copper electrode was found to be 1.39×10^{-8} mol cm^{-2},[55] and the surface coverage concentration of poly[Ni^{II}-BA] was calculated as 2.1×10^{-8} mol cm^{-2},[54] which indicated that Ag_2O NWA/CRIE owns much larger surface coverage, so it has a bigger area to come into contact with that tested.

Figure 5c shows the amperometric response of Ag_2O NWA/CRIE at 0.37 V. According to the changes of the HZ concentration by successively added HZ in 0.1 M NaOH, the electrode responds sensitively, reaching a steady-state signal within 3 s, and is linear in the HZ concentration range of 0.2−1270 μM with a sensitivity of 660.3 μA mM^{-1}, as depicted in the inset picture of Figure 5c. Exhilaratingly, the electrode also shows a low detection limit of 0.01 μM (S/N = 3) toward the detection of HZ; the detection limit of different electrodes was compared to that of Ag_2O NWA/CRIE, which is shown in Table S1 in the Supporting Information.

It is well-known that dopamine (DA), ascorbic acid (AA), and L-cysteine (L-Cys) are common interfering species in physiological samples. Thus, we conducted the interference test by measuring the current changes caused by the addition of DA, AA, and L-Cys. An amperometric response was obtained by the successive injection of 0.02 mM HZ and interfering species (0.1 mM DA, 0.1 mM AA, and 0.1 mM L-Cys). As shown in Figure 5d, an obvious current response was observed when 0.02 mM HZ was added; on the contrary, no obvious current response was observed with the consecutiveaddition of 0.1 mM AA, 0.1 mM DA, and 0.1 mM L-Cys, which demonstrated that the electrode can completely avoid interference from the interfering species.

3.4. Potential Application in the HZ Fuel Cell. In order to investigate the catalytic performance of Ag_2O NWA, an integrated electrode was also used as an electrocatalyst in the HZ fuel cell. Figure 6a shows the electrochemical behavior in a 3 M NaOH solution with and without HZ for a bare Cu rod. For a solution without HZ, the LSV curve reveals that the copper begins to be oxidized when the potential is −0.55 V. After 0.5 M or 1 M HZ was added to the solution, we observed the LSV curve, the potential of the anodic peak of which is around −0.58 V. As a result, there is a linear relationship between the current value at this peak and the concentration of HZ, and the evident anodic peak should be due to oxidation of HZ. As we know, when the potential is set as more positive than −0.55 V, the copper could be oxidized and potential corrosioncould have a negative effect on the catalytic performance of Ag_2O NWA, so setting the maximum potential at −0.6 V in the following LSV should be the solution. Figure 6b is a comprehensive figure showing the catalytic performance on electrodes of Ag_2O NWA, Ag_2O nanowalls, a bare Cu rod, and ordinary silver electrodes in a 3 M NaOH solution with 1 M N_2H_4. At −0.6 V, no apparent current was obtained on an ordinary silver (polycrystalline silver) electrode, but there was considerable current (3.9 mA cm^{-2}) on a bare Cu electrode, which implied that bare Cu owns a catalytic performance superior to that of silver on the aspect of oxidation of HZ. In contrast, the current density of Ag_2O nanowalls is just 62.4 mA cm^{-2}. The anodic current density increased quickly as Ag_2O NWA was synthesized on the Cu rod and was almost 25 times (reaching 94.4 mA cm^{-2}) higher than that on bare Cu and 1.5 times higher than that on Ag_2O nanowalls. We did further research to study the size effect of the Ag_2O nanowires on the catalytic activity of HZ; Figure S9 in the Supporting Information shows that the size of the Ag_2O nanowires can affect the catalytic activity of HZ. The current densities of the Ag_2O nanowires of parts c,d and e,f of Figure 4 are 76.3 and 42.8 mA cm^{-2}, respectively; compared with 94.4 mA cm^{-2}, the current density seems to be weak. The Ag_2O nanowires of Figure 1a,b show better catalytic activity of HZ.

For comparison of the performances of the catalysts, the onset oxidation potential (E_{on}) of HZ is regarded as an evaluation criterion. We can see the inset graph in Figure 6b. E_{on} on Ag_2O NWAs (−0.85 V) was lower than those on a bare Cu rod (−0.76 V) and Ag_2O nanowalls (−0.82 V). The evident 90 and 30 mV negative potential shifts revealed that Ag_2O NWAs not only possess superior oxidation ability toward to HZ but also can work at more negative potential. The E_{on} values of other materials are summarized in Table S2 in the Supporting Information. As a result, Ag_2O NWAs have potential applications in the HZ fuel cell.

Ag_2O NWAs have higher catalytic performance than Ag_2O nanowalls, which may be due to their electrochemical active surface (EAS). To prove this, the EAS of the two electrodes was measured by means of CV in 0.1 M NaOH. The peaks in the potential region −800 mV < E < −500 mV on the CV curve are associated with the hydrogen adsorption process in the anodic scan.[56] The EAS is calculated according to the equation[57]

$$\mathrm{EAS} = \frac{4.76Q_H}{[\mathrm{MO}]}$$

where Q_H denotes the Coulombic charge for hydrogen desorption at the electrodes (mC cm^{-2}) and [MO] represents nanomaterial (Ag_2O NWAs or Ag_2O nanowalls) loading (mg cm^{-2}) on the electrode. The EAS for Ag_2O NWAs is 23.8 cm^2 g^{-1}, and that for Ag_2O nanowalls is 15.7 cm^2 g^{-1}. The results confirmed that the EAS for Ag_2O NWAs is bigger than that for Ag_2O nanowalls, which verifies our estimation.

4. CONCLUSION

A novel Ag_2O NWA nanostructure was successfully fabricated on a Cu rod. The study showed that this Ag_2O NWA is grown from the former silver layered film. The integrated electrode (Ag_2O NWA/CRIE) showed excellent performance on the detection of HZ, so it can potentially be used in some novel electrochemical sensors and other electronic devices. Satisfactorily, we found that Ag_2O NWAs have a superior catalytic performance; this special Ag_2O NWA material could be a applicable candidate as a catalyst in the HZ fuel cell.

■ ASSOCIATED CONTENT

Supporting Information

XRD and EDX patterns of the Ag_2O NWA, XPS spectra of Ag 3d for Ag_2O, typical SEM images of the product of the contrast experiment and the corresponding EDX of the product, cyclic voltammograms, comparison of the performances of amperometric HZ sensors based on different modified electrode materials, size effect of Ag_2O nanowires on the catalytic activity of HZ, and comparison of other materials based on the onset oxidation potential. This material is available free of charge via the Internet at http://pubs.acs.org.

■ AUTHOR INFORMATION

Corresponding Authors

*E-mail: wangyuz@mail.ahnu.edu.cn.
*E-mail: xjzhang@mail.ahnu.edu.cn.

Notes

The authors declare no competing financial interest.

■ ACKNOWLEDGMENTS

This work was financially supported by the National Natural Science Foundation of China (Grants 21073001 and 21005001), Key Project of Chinese Ministry of Education (Grant 209060), Anhui Provincial Natural Science Foundation (Grant 1208085QB28), Natural Science Foundation of Anhui (Grant KJ2012A139), and the Program for Innovative Research Team at Anhui Normal University.

■ REFERENCES

(1) Zhang, Z. C.; Zhang, X.; Yu, Q. Y.; Liu, Z. C.; Xu, C. M.; Gao, J. S.; Zhuang, J.; Wang, X. *Eur. J. Chem.* **2012**, *18*, 2639−2645.
(2) Mu, Y.; Jia, D. L.; He, Y. Y.; Miao, Y. Q.; Wu, H. L. *Biosens. Bioelectron.* **2011**, *26*, 2948−2952.
(3) Wang, N.; Cao, X.; Chen, Q. J.; Lin, G. *Eur. J. Chem.* **2012**, *18*, 6049−6054.
(4) Sun, Y. G. *J. Phys. Chem. C* **2010**, *114*, 2127−2133.
(5) Wang, N.; Yao, B. D.; Chan, Y. F.; Zhang, X. Y. *Nano Lett.* **2003**, *3*, 475−477.
(6) Jung, H. S.; Hong, Y. J.; Li, Y. R.; Cho, J. H.; Kim, Y. J.; Yi, G. C. *ACS Nano* **2008**, *2*, 637−642.
(7) Schneider, J. J.; Engstler, J.; Franzka, S.; Hofmann, K.; Albert, B.; Ensling, J.; Guttlich, P.; Hildebrandt, P.; Dopner, S.; Pfleging, W.; Gunther, B.; Muller, G. *Eur. J. Chem.* **2001**, *7*, 2888−2895.
(8) Ding, L. X.; Li., G. R.; Wang, Z. L.; Lin, Z. Q.; Liu, H.; Tong, Y. X. *Eur. J. Chem.* **2012**, *18*, 8386−8391.
(9) Liu, B. D.; Bando, Y.; Tang, C. C.; Xu, F. F.; Golberg, D. *J. Phys. Chem. B* **2005**, *109*, 21521−21524.
(10) Wang, C.; Daimon, H.; Lee, Y. G.; Kim, J.; Sun, S. H. *J. Am. Chem. Soc.* **2007**, *129*, 6974−6975.
(11) Wu, H. B.; Chen, W. *J. Am. Chem. Soc.* **2011**, *133*, 15236−15239.
(12) Wang, X.; Li, Y. D. *Eur. J. Chem.* **2003**, *9*, 5627−5635.
(13) Tian, Q. Y.; Shi, D. X.; Sha, Y. W. *Molecules* **2008**, *13*, 948−957.
(14) Wang, X. F.; Li, S. F.; Yu, H. G.; Yu, J. G.; Liu, S. W. *Eur. J. Chem.* **2011**, *17*, 7777−7780.
(15) Wang, X.; Wu, H. F.; Kuang, Q.; Huang, R. B.; Xie, Z. X.; Zheng, L. S. *Langmuir* **2010**, *26*, 2774−2778.
(16) Murray, B. J.; Li, Q.; Newberg, J. T.; Hemminger, J. C.; Penner, R. M. *Chem. Mater.* **2005**, *17*, 6611−6618.
(17) Zhang, Q. M.; Li, Y.; Xu, D. S.; Gu, Z. N. *J. Mater. Sci. Lett.* **2001**, *20*, 925−927.
(18) Gallardo, O. A. D.; Moiraghi, R.; Macchione, M. A.; Godoy, J. A.; Perez, M. A.; Coronado, E. A.; Macagno, V. A. *RSC Adv.* **2012**, *2*, 2923−2929.
(19) Zou, J.; Xu, Y.; Hou, B.; Wu, D.; Sun, Y. H. *Powder Technol.* **2008**, *183*, 122−126.
(20) Lyu, L. M.; Huang, M. H. *J. Phys. Chem. C* **2011**, *115*, 17768−17773.
(21) Fang, J. X.; Leufke, P. M.; Kruk, R.; Wang, D.; Scherer, T.; Hahn, H. *Nano Today* **2010**, *5*, 175−182.
(22) Kawasaki, M.; Nishimura, N. *J. Phys. Chem. C* **2008**, *112*, 15647−15655.
(23) Yan, Z. J.; Bao, R. Q.; Chrisey, D. B. *Langmuir* **2011**, *27*, 851−855.
(24) Wang, G. F.; Gu, A. X.; Wang, W.; Wei, Y.; Wu, J. J.; Wang, G. Z.; Zhang, X. J.; Fang, B. *Electrochem. Commun.* **2009**, *11*, 631−634.
(25) Zheng, L.; Song, J. F. *Talanta* **2009**, *79*, 319−326.
(26) Zhang, F.; Zhang, L.; Xing, J. F.; Tang, T. H.; Xia, X. H. *ChemPlusChem* **2012**, *77*, 914−922.
(27) Rosca, V.; Koper, M. T. M. *Electrochim. Acta* **2008**, *53*, 5199−5205.
(28) Umar, A.; Rahman, M. M.; Kim, S. H.; Hahn, Y. B. *Chem. Commun.* **2008**, *44*, 166−168.
(29) Zhao, J.Y.; Zhu, M. N.; Zheng, M.; Tang, Y. W.; Chen, Y.; Lu, T. H. *Electrochim. Acta* **2011**, *56*, 4930−4936.
(30) Gao, G. Y.; Guo, D. J.; Wang, C.; Li, H. L. *Electrochem. Commun.* **2007**, *9*, 1582−1586.
(31) Li, J.; Lin, X. Q. *Sens. Actuators, B* **2007**, *126*, 527−535.
(32) Liang, Y.; Zhou, Y.; Ma, J.; Zhao, J. Y.; Chen, Y.; Tang, Y. W.; Lu, T. H. *Appl. Catal. B: Environ.* **2011**, *103*, 388−396.
(33) Yang, H. D.; Zhong, X.; Dong, Z. P.; Wang, J.; Jin, J.; Ma, J. T. *RSC Adv.* **2012**, *2*, 5038−5040.
(34) Gao, H. C.; Wang, Y. X.; Xiao, F.; Ching, C. B.; Duan, H. W. *J. Phys. Chem. C* **2012**, *116*, 7719−7725.
(35) Evans, G.; Kordesch, K. *Science* **1967**, *158*, 1148−1152.
(36) Fleischmann, M.; Korinek, K.; Pletcher, D. *J. Electroanal. Chem.* **1972**, *34*, 499−503.
(37) Broussely, M.; Goudeau, J. C.; Bernard, M. L. *Electrochim. Acta* **1975**, *20*, 233−236.
(38) Korovin, N. V.; Yanchuk, B. N. *Electrochim. Acta* **1970**, *15*, 569−580.
(39) Otomo, M.; Nakayama, I. *Microchem. J.* **1980**, *25*, 75−81.
(40) Burke, L. D.; Moynihan, A. *Electrochim. Acta* **1981**, *16*, 167−171.
(41) Kodera, T.; Honda, M.; Kita, H. *Electrochim. Acta* **1985**, *30*, 669−675.
(42) Aggarwal, R. C.; Narang, K. K. *Inorg. Chim. Acta* **1973**, *7*, 651−652.
(43) Issa, Y. M.; Zaky, M. *Microchem. J.* **1986**, *33*, 126−131.
(44) Clark, A. J.; Pickering, W. F. *J. Inorg. Nucl. Chem.* **1969**, *21*, 319−327.

(45) Korinek, K.; Koryta, J.; Musilova, M. *J. Electroanal. Chem. Interfacial Electrochem.* **1969**, *21*, 319−327.
(46) Granota, E.; Filanovsky, B.; Presman, I.; Kuras, I.; Patolsky, F. *J. Power Sources* **2012**, *204*, 116−121.
(47) Yin, W. X.; Li, Z. P.; Zhu, J. K.; Qin, H. Y. *J. Power Sources* **2008**, *182*, 520−523.
(48) Chinchilla, J. S.; Asazawa, K.; Sakamoto, T.; Yamada, K.; Tanaka, H.; Strasser, P. *J. Am. Chem. Soc.* **2011**, *133*, 5425−5431.
(49) Asazawa, K.; Yamada, K.; Tanaka, H.; Taniguchi, M.; Oguro, K. *J. Power Sources* **2009**, *191*, 362−365.
(50) Kubo, D.; Tadanaga, K.; Hayashi, A.; Tatsumisago, M. *J. Power Sources* **2013**, *222*, 493−497.
(51) Serov, A.; Kwak, C. *Appl. Catal. B: Environ.* **2010**, *98*, 1−9.
(52) Lao, S. J.; Qin, H. Y.; Ye, L. Q.; Liu, B. H.; Li, Z. P. *J Power Sources* **2010**, *195*, 4135−4138.
(53) Zhang, X. J.; Ji, R.; Wang, L. L.; Yu, L. T.; Wang, J.; Geng, B. Y.; Wang, G. F. *CrystEngComm* **2013**, *15*, 1173−1178.
(54) Zheng, L.; Song, J. F. *Talanta* **2009**, *79*, 319−326.
(55) Nezhad, G. K.; Jafarloo, R.; Dorraji, P. S. *Electrochim. Acta* **2009**, *54*, 5721−5726.
(56) Eileen, H. Y.; Scott, K.; Reeve, R. W. *J. Electroanal. Chem.* **2003**, *547*, 17−24.
(57) Xu, C. W.; Shen, P. K. *Chem. Commun.* **2004**, *19*, 2238−2239.